

### International Journal of Design & Nature and Ecodynamics

Vol. 20, No. 9, September, 2025, pp. 2157-2165

Journal homepage: http://iieta.org/journals/ijdne

# Green Synthesis of Star Anise (*Illicium verum*)-Mediated Manganese Oxide Nanocomposite for Efficient Pb(II) and Cr(VI) Adsorption



Qater Al-Nada Ali Kanaem Al-Ibady

Department of Medical Laboratory Technology, College of Health and Medical Techniques, Middle Technical University (MTU), Baghdad 10098, Iraq

Corresponding Author Email: drqateralnada@mtu.edu.iq

Copyright: ©2025 The author. This article is published by IIETA and is licensed under the CC BY 4.0 license (http://creativecommons.org/licenses/by/4.0/).

https://doi.org/10.18280/ijdne.200919

Received: 9 July 2025 Revised: 16 August 2025 Accepted: 22 August 2025

Available online: 30 September 2025

#### **Keywords:**

environmental remediation, green synthesis, nanocomposites, nanoparticles, star anise, Illicium verum

#### **ABSTRACT**

Green-synthesized nanocomposites offer a sustainable solution for water purification, addressing the environmental risks associated with heavy metal pollution from lead and chromium. This study investigated the green synthesis of a manganese oxide nanocomposite (MnO@SE) using star anise (Illicium verum) extract for efficient adsorption of Pb(II) and Cr(VI). MnO@SE was synthesized using Illicium verum extract and characterized using different spectroscopic techniques. Batch adsorption experiments optimized pH, dosage, contact time, and concentration for Pb(II) and Cr(VI) elimination. The characterization revealed high crystallinity, spherical morphology (~80 nm), a BET surface area of 157 m<sup>2</sup>/g, and a zeta potential of 2.1 mV, indicating stability and a favorable surface charge for adsorption. Batch adsorption experiments optimized parameters, including pH (2.0) for Cr(VI) and Pb(II), adsorbent dosage (0.6 g), contact time (50 min), and initial metal concentration (25 mg/L). Under optimal circumstances, the MnO@SE achieved maximum adsorption capacities of 25 mg/g for Pb(II) and 25 mg/g for Cr(VI) in single-metal systems, with removal efficiencies of 99.6% and 94.26%, respectively. The MnO@SE nanocomposites showed higher affinity in single-metal systems, proving their applicability for sustainable heavy-metal remediation, though further research should focus on regeneration performance and real-wastewater testing.

### 1. INTRODUCTION

As a result of their toxicity, persistence, and bioaccumulative nature, heavy metal poisoning tends to cause significant hazards to public health and the environment, especially when it comes to lead (Pb2+) and hexavalent chromium (Cr<sup>6+</sup>). Notably, these sorts of contaminants, which are basically obtained from industrial processes including mining, battery production, and electroplating, can infiltrate water bodies and cause detrimental effects on the ecosystem and human well-being as well [1]. However, attendant low efficiency noticed at low contaminant concentrations, secondary pollutant formation, and high running costs are common drawbacks of traditional remediation technologies, such as chemical precipitation and ion exchange. On account of this, there is a growing need for highly effective, sustainable, and reasonably priced methods to reduce heavy metal contamination in aquatic settings [2, 3].

Therefore, premised on its ease of use, efficiency, and adaptability, adsorption has proven to be a successful method for purifying water. To limit the influence on the environment, recent research has focused on creating nanocomposite materials that are created by green synthesis, using biological components as stabilizers and reducing agents for nanoparticles. In a bid to provide evidence for the credibility of such green-synthesized materials in heavy metal removal,

Aziz et al. [4] represented the synthesis of organically modified bentonites-ZnO nanoparticle nanocomposite (OB/ZnO) with adsorption capacities of 460.31 mg/g for Cr and 407.6 mg/g for Pb(II) ions. Nonetheless, Wei et al. [5] showed a higher adsorption capacity of Pb(II) ions from tainted water using a green nanocomposite obtained from a polymer through the introduction of CuO nanoparticles and polyaniline (PANI). In this light, for the purpose of improving the adsorption efficiency, this study emphasized the necessity for adjusting variables, such as pH and adsorbent dose, and starting ion concentration. A lignosulfonate-graphene oxide porous hydrogel nanocomposite (LGPH) has been created using an environmentally friendly method [6]. Since these conventional methods could cause harmful impacts on the ecosystem, it is necessary to enhance the ambient environment to allow bacterial remediation [1]. The application of resistant natural techniques is a workable substitute for biological remediation. Therefore, it is evident that the adoption of resistant bacteria may make it possible to create efficient methods for eliminating heavy metals from the environment as part of initiatives to create a sustainable ecosystem [2, 3]. It has adsorption capabilities of 283.2 mg/g for Pb(II) ions and 142.25 mg/g for Cr ions. The LGPH nanocomposite also exhibited excellent reusability with retained uptake capacity over multiple reuse cycles, demonstrating its potential for practical uses in the purification of water.

Green synthesis of nanocomposites is the application of green methods, i.e., employing plant extracts, microbes, or biopolymers, to produce nanomaterials without the use of any poisonous chemicals. Green synthesis through plant extract, for instance, employs phytochemicals as reductive and capping agents in nanomaterial formation. When using intracellular or extracellular methods, microbial species, including bacteria and fungi, also participate in the creation of nanocomposites. Because of their functional qualities and biocompatibility, these techniques are becoming more popular in medicine delivery, agriculture, and environmental cleanup [7, 8]. The concept of sustainable chemistry and the convergence of nanotechnology are aligned with the synthesis of nanocomposites through environmentally approaches. Green synthesis offers green, affordable, and biocompatible alternatives to traditional methods, reducing toxic waste and energy use. Unlike conventional chemical synthesis, which often relies on hazardous reagents and generates pollution, green approaches use renewable resources under mild conditions. Green synthesis reduces energy consumption by operating under ambient temperature and pressure, unlike conventional methods requiring high heat or pressure [7, 8]. It avoids hazardous chemicals, lowering environmental and health risks [9]. However, despite their eco-safety, comprehensive toxicity assessments of greensynthesized nanomaterials remain limited [10]. However, challenges remain in scalability, reproducibility, and mechanistic control, requiring further optimization for industrial adoption. Future research and better care are essential to safeguarding the environment and public health [2, 3].

Therefore, the present research investigated the potential of green-synthesized nanocomposite materials for the adsorption of heavy metals to offer economical and ecologically friendly alternatives to conventional methods. By using green synthesis and characterization, this study also aims to develop a novel nanocomposite for the efficient adsorption of Pb(II) and Cr(VI) for environmental remediation.

### 2. MATERIALS AND METHODS

#### 2.1 Sources of chemicals and plant material

All the reagents employed to conduct these experiments, including manganese (II) acetate tetrahydrate and butyl carbitol acetate (BCA), were analytical grade and purchased from Merck and Aldrich (Darmstadt, Germany). In addition, dry star anise fruit (*Illicium verum*) was also purchased from a local grocery vendor (Al-Sadriya Market).

### 2.2 Methods

### 2.2.1 Stock solution preparation

To create stock solutions for adsorption investigations of Cr(VI) and Pb(II) ions in deionized water, potassium dichromate (K<sub>2</sub>Cr<sub>2</sub>O<sub>7</sub>) and lead sulfate (PbSO<sub>4</sub>) were dissolved. In particular, the stock solution was made by dissolving 100 mg of each component in 1 L of distilled water.

#### 2.2.2 Preparation of plant extract

In a flask, 50 mL of deionized water was mixed with 2 g of powdered star anise (*Illicium verum*) and heated for two minutes to create manganese oxide (MnO) nanoparticles.

After stirring and cooling, the mixture was centrifuged for ten minutes at 7,500 rpm. The star anise extract (SE), which was identified as the clear supernatant, was gathered and kept at 4°C.

### 2.2.3 Green synthesis of manganese oxide nanoparticles with star anise

To synthesize MnO nanoparticles, a modified method from study [11] was used. An aliquot of 40 mM aqueous solution of manganese acetate (II) tetrahydrate was combined with 1 mL of SE (Figure 1). For 24 and 72 hours, the mixture was incubated at 25°C. Various physicochemical parameters were varied to synthesize MnO nanoparticles of different sizes, including metal ion concentrations, SE concentrations, metal ion volumes, and incubation temperature. The metal ion concentration was systematically changed from 1 to 80 mM, and 1mL of each concentration was incubated with 1mL of SE. The volume of SE was changed from 0.25 to 1 mL. Besides, by adjusting the SE volume from 1 to 4 mL and the metal ion volumes from 1 to 5 mL at a fixed volume of metal ions of 1 mL, the impact of metal ion volume on the yield and particle size of MnO nanoparticles was examined. By incubating 1 mL of 40 mM metal ion solution with 1mL of SE under incubation conditions between 25 and 85°C, the impacts of temperature on the characteristics of nanoparticles were ascertained.



**Figure 1.** Diagrammatic green production of manganese nanoparticles with fruit extract from star anise

### 2.2.4 Determination of nanocomposite zero point of charge

To ascertain the zero point of charge (pH<sub>zpc</sub>) values of manganese oxide nanoparticles synthesized using SE (MnO@SE), 0.1 grams of all samples were blended with 50mL of a 0.1 M NaCl solution [12], ranging from an initial pH (2 to 11). The mixture was shaken vigorously for two days. After allowing the samples to settle, the pH values at equilibrium were determined. The starting pH values of the solution were graphed against its initial and equilibrium pH values. Following the procedures outlined in the relevant literature, the pH<sub>zpc</sub> value was established at the graph's x-axis point of intersection.

# 2.2.5 Characterization of green-synthesized manganese oxide nanoparticles

Using ultraviolet-visible (UV-Vis) spectroscopy, the synthesis of MnO@SE was confirmed. Adsorbents were subjected to Fourier transform infrared (FTIR) spectroscopy, which has a 400-4000cm<sup>-1</sup> scanning range. A transmission electron microscope (JEOL TTM-2110, UK) was utilised to measure the nanoparticle sizes. Employing a Quanta 250 instrument equipped with an EDX detector, scanning electron

microscopy (SEM) images were obtained. X-ray diffraction (XRD) at a wavelength of  $\lambda$ =1.54 Å was used. A digital pH meter (45880IDS, SES, Germany) was used to measure the pH. The crystallite size from X-ray (XRD) peaks was estimated using a modified Scherrer equation [13], as shown in Eq. (1).

$$\ln \beta = \ln \left( \frac{K\lambda}{D} \right) - \ln \left( \cos \theta \right) \tag{1}$$

where,  $\beta$  is the FWHM of the diffraction peak (in radians) after instrumental correction, K is the shape factor (commonly 0.9),  $\lambda$  is the X-ray wavelength (nm), D is the crystallite size (nm), and  $\theta$  is the Bragg angle (radians).

### 2.2.6 Adsorption isotherm and kinetic models

To represent the interaction of Pb(II) and Cr(VI) with MnO@SE, the Freundlich and Langmuir isotherm models were used to match the adsorption data. The Freundlich model takes into account multilayer adsorption on heterogeneous surfaces, while the Langmuir model assumes monolayer adsorption on a homogeneous surface. Their mathematical forms are:

$$\text{Langmuir model: } q_e = \frac{q_m b C_e}{1 + b C_e}$$

Freundlich model: 
$$q_e = K_F C_e^{1/n}$$

where, the Langmuir constant is b (L mg<sup>-1</sup>), the equilibrium adsorption quantity is  $q_e$  (mg g<sup>-1</sup>), the equilibrium concentration of Pb(II) or Cr(VI) is  $C_e$  (mg L<sup>-1</sup>), and the maximal adsorption capacity is  $q_m$ ,  $K_F$  is the Freundlich constant, and n represents adsorption intensity.

For kinetic modeling, the adsorption behavior of Pb(II) and Cr(VI) was evaluated using pseudo-first-order and pseudo-second-order models:

Pseudo-first-order: 
$$q_t = q_e(1-e^{-k1t})$$

Pseudo-second-order: 
$$q_t = \frac{q_e^2 k_2 t}{1 + q_e k_2 t}$$

where, adsorption capacities represented by  $q_e$  and  $q_t$  at time t and equilibrium, respectively, while  $k_1$  (min<sup>-1</sup>) and  $k_2$  (g mg<sup>-1</sup> min<sup>-1</sup>) are the rate constants for the respective models.

### 3. RESULTS AND DISCUSSION

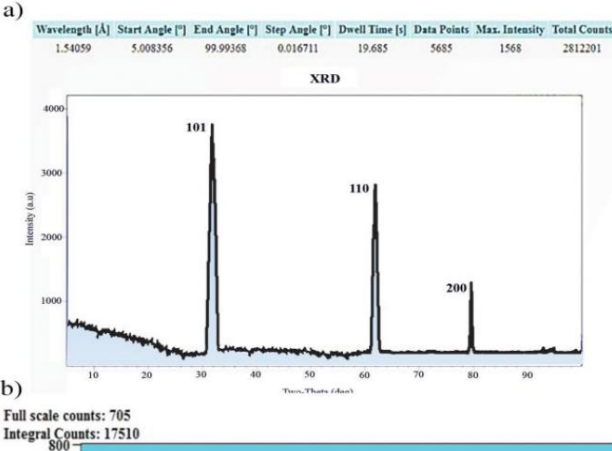
# 3.1 Adsorbent properties determined by X-ray diffraction analysis

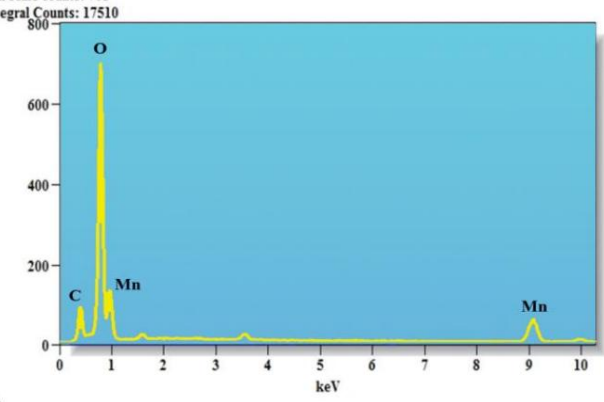
Figure 2(a) shows the green-synthesized MnO@SE nanoparticles' X-ray diffraction (XRD) pattern. The diffraction is indicative of sharp diffraction peaks at the 101, 110, and 200 crystal planes at 38°, 44°, and 56°, respectively [14]. The exceptionally high crystallinity of the produced particles was further confirmed by the maximum peak intensity and sharpness at the 101 plane at 37°. Notably, the XRD pattern's lack of impurity peaks indicates that the MnO@SE nanoparticles are pure.

# 3.2 Adsorbent properties determined via energy dispersive X-ray analysis (EDX)

Green-synthesized MnO@SE nanoparticles' chemical

formation and synthesis were ascertained using EDX analysis. As shown in Figure 2(b), the EDX spectrum exhibits a strong manganese (Mn) peak at approximately 0.71 keV, directly confirming the presence of Mn in the prepared nanoparticles [15]. Additional peaks corresponding to oxygen (O) and carbon (C) are also evident, indicating the adsorption of biological compounds from the star anise extract onto the nanoparticle surface. Importantly, the EDX profile shows no extraneous peaks related to impurities, further supporting the purity and successful one-pot green synthesis of the nanoparticles by the plant extract [16]. These results align well with previously reported studies concerning biosynthesized metal oxide nanoparticles.





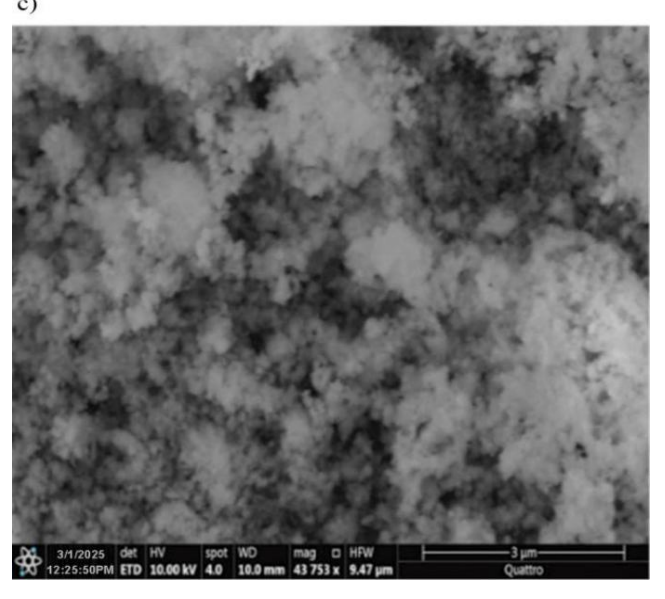


**Figure 2.** Green-synthesized manganese oxide nanoparticle characterization by energy-dispersive (a) X-ray diffraction spectra; (b) EDX analysis; and (c) SEM micrographs

# 3.3 Adsorbent properties determined by scanning electron microscopy analysis

MnO@SE nanoparticles' size was determined by scanning electron microscopy (SEM) analysis. The SEM picture in Figure 2(c) shows that the MnO@SE nanoparticles are spherical in shape. Additionally, the nanoparticles are widely distributed. As can be observed from Figure 3(a), the particle size distribution is right-skewed. Particle size distribution analysis revealed that the average particle size of the produced MnO@SE nanoparticles is approximately  $80 \pm 0.5$  nm.

# 3.4 Characteristics of adsorbent based on the UV-Vis spectrometry and FTIR analysis

To study the various functional groups and absorption of the biomolecules in the star anise fruit extract for reduction and capping processes, the MnO@SE nanoparticles and plant extract were examined using UV-visible and FTIR. The UV-visible scan indicated that the fruit extract of the plant exhibited maximum absorption in the 200-390 nm range of UV, indicating that it contains strong polyphenols and

flavonoids that absorb UV radiation because of the presence of hydroxyl (OH) groups [17] with two noticeable signals, at 380 nm (due to biochemical phytomolecules) and 460 nm (due to Mn-O), the biogenic MnO@SE nanoparticles displayed a broad absorption band (Figure 3(a)). The Mn-O absorption maximum was slightly red-shifted compared to the previously reported value [18], and can be attributed to transferring phytomolecules' non-bonding electrons to manganese's empty d-orbitals, which facilitates electron transitions and causes a redshift of the absorption maximum to longer wavelengths [19]. The plant extract contains a variety of biological constituents with different functional groups, according to the FTIR spectrum. The functional groups were consistent with the previously obtained functional groups. In greensynthesized MnO@SE nanoparticles, FTIR characteristic peaks for Mn-O at approximately 580 cm<sup>-1</sup> were noticed, along with O-H, C=O, N-H, and C-O peaks [20]. FTIR peak was as documented in the literature, confirming that the plant extract's physiologically active phytomolecules with these functional groups cap the MnO@SE nanoparticles (Figure 3(b)).

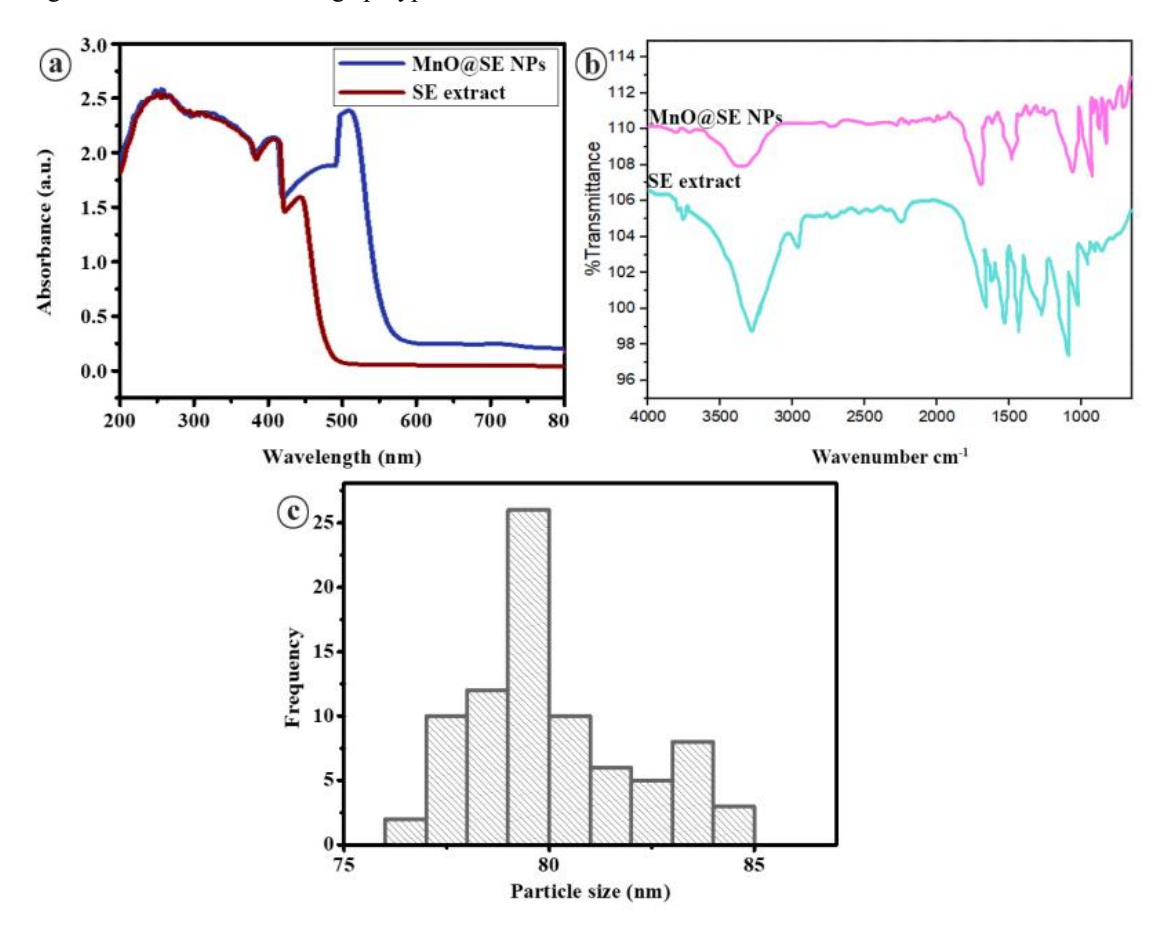


**Figure 3.** (a) Ultraviolet-visible spectra, (b) Fourier-transform infrared spectroscopy spectra, and (c) Particle-size distribution based on transmission electron microscopy of green-synthesized manganese oxide nanoparticles

### 3.5 Proposed mechanism for the synthesis

The literature has demonstrated that star anise fruit extract contains a wide range of physiologically active phytochemical compounds, including lignin, fixed and volatile oils, carbohydrates, steroids, terpenoids, tannins, saponins, flavonoids, phenolics, alkaloids, proteins, anthraquinones, and cardiac glycosides (Figure 4). These compounds occur in the plant extract as well as in the produced nanoparticles,

supported by UV-visible and FTIR spectra. These are thought to function as capping and reducing agents when MnO@SE nanoparticles are formed. Particularly, in synthesis, phytochemicals like flavonoids, phenolics, and carbohydrates act as electron donors to convert manganese ions (Mn<sup>+</sup>) into their elemental form (Mn<sup>0</sup>) through a redox reaction. Other chemicals, including alkaloids and proteins, cap the Mn<sup>0</sup> species to stabilize them, as shown in Figure 4. Plant extract-mediated synthesis of nanoparticles has been documented in

recent literature [21].



**Figure 4.** Manganese oxide nanoparticle synthesis process employing star anise extract

### 3.6 Investigations of the batch adsorption of manganese oxide nanoparticles made with star anise extract

Using manganese oxide nanoparticles loaded with SE and

produced by green synthesis, batch adsorption studies were assessed to determine the ideal conditions for precipitating the metal ion. The process of adsorption efficiency was examined as a function of a varied set of parameters, like concentration of metal-ion effluent, amount of adsorbent, solution pH, and duration of contact between metal ions and adsorbent (Figure 5).

#### 3.6.1 Effect of metal ion concentration

Maximum adsorption efficiencies were found at 25 mg/L, where they were 94.54% for Pb(II) and 98.37% for Cr(VI), after adsorption efficiency was examined at different starting metal ion concentrations. Adsorption efficiency decreased when the starting concentration was raised above 25 mg/L. This decrease was because of the limited accessibility of sites on the MnO@SE surface [22], which restricted further adsorption. This shows that while the most appropriate concentration for subsequent experiments was found to be 25 mg/L, there was still capacity for further adsorption at lower concentrations (Figure 5(a)). Notably, the adsorbent's performance was distinctly different in multi-metal and singlemetal systems. In single-metal systems, efficiency in adsorption was higher due to the exclusive existence of suitable active sites for the respective metal ions. On the other hand, in multi-metal systems, competition among active sites lowered each ion's efficiency of adsorption [23].

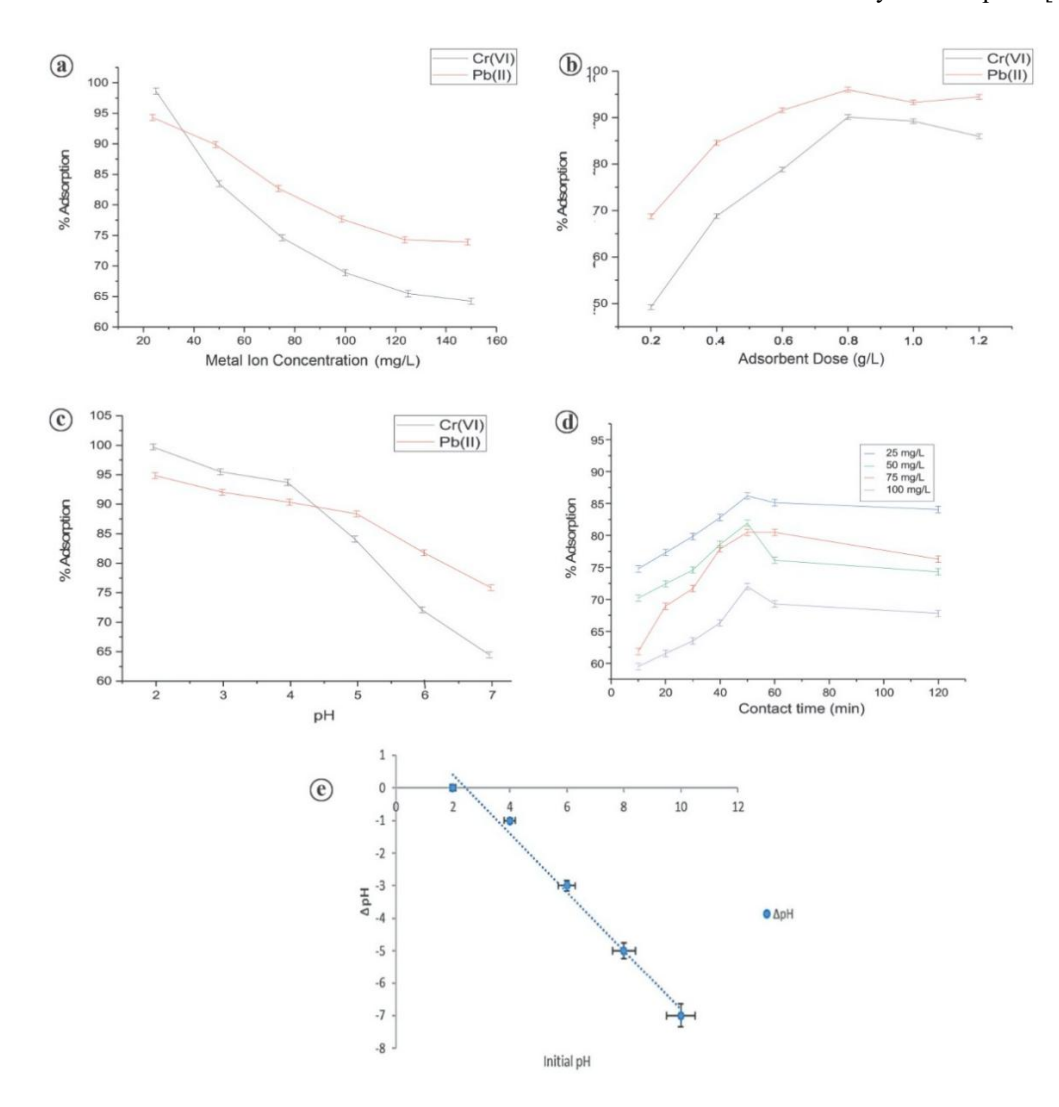


**Figure 5.** Batch mode of adsorption studies on manganese oxide nanoparticles synthesized using star anise extract. (a) adsorbent dose; (b) ion concentration; (c) pH; (d) contact time; (e) pH<sub>zpc</sub>

#### 3.6.2 Effect of dose on metal ions

The doses of MnO@SE had a substantial impact on how well metal ions were adsorbed by the material. While maintaining the pH at the optimal level of 2.0, different dosages of MnO@SE, ranging from 0.2 to 0.8 mg/L, were investigated in a batch test. The initial metal ion value for the test was 50 mg/L, and it was conducted at room temperature. First, the increase in dosage of MnO@SE nanoparticles led to enhanced adsorption capacity since there are more active sites available [24]. When the dosage was more than 0.6 mg/L, however, a reduction of adsorption efficiency was noted, which suggests that the active sites were nearing saturation (Figure 5(b)).

### 3.6.3 Effect of pH on metal ions

With the aid of HNO<sub>3</sub>, pH was changed and maintained constant to evaluate the adsorption capacity of Pb(II) and Cr(VI) under batch conditions. Experiments were carried out using 25 mg/L of ion concentration, an adsorbent dosage of 0.2 g, and 60 min of contact time at room temperature (25°C). Adsorption efficiency for both Pb(II) and Cr(VI) appeared to be highest at pH 2.0, achieving 96.8% and 99.6% removal, respectively (Figure 5(c)). At higher pH values, adsorption efficiency decreased due to the reduction in electrostatic attraction between the positively charged metal ions and the MnO@SE surface. Additionally, deprotonation of surface functional groups at higher pH decreases the quantity of binding sites that are available. In strongly acidic conditions, hydronium ions (H<sub>3</sub>O<sup>+</sup>) also compete with Pb(II) and Cr(VI) for adsorption sites, but despite this competition, the surface chemistry of MnO@SE favored adsorption at pH 2.0, making it the most suitable pH for maximum removal efficiency [25].

### 3.6.4 Duration of contact's impact on metal ions

The length of time the adsorbent and adsorbents were in contact was crucial to the adsorption process. At room temperature, the 10–120-minute contact duration was examined with an adsorbent dose of 0.2 g/L and an ideal pH of 2.0. As contact time increased, the rate of Cr(VI) and Pb(II) ion adsorption rose as well, peaking at 50 minutes. For longer than that, the adsorbent's accessible active sites shrank, reducing its adsorption capability. This saturation resulted in most active sites being covered by metal ions [26], and the uptake rate therefore decreased (Figure 5(d)).

### 3.6.5 Effect of the zero point of charge on metal ions

Solution pH has an important bearing on the calculation of the adsorbent's surface charge and thus its ability to adsorb. The prepared star anise nanoparticles had a zero-point charge value of about 2.1 (Figure 5(e)). As pH crosses this threshold, the nanoparticle surface gains a negative charge, and the adsorption of Cr(VI) and Pb(II) is enhanced [27]. Conversely, at lower pH than the pH<sub>zpc</sub>, the surface is positive, and cation adsorption decreases and anion adsorption increases instead [27]. Understanding the pH<sub>zpc</sub> is important for condition optimization for optimizing adsorbents to achieve optimum efficiency under current environmental circumstances in order to effectively remove metal ions by star anise-derived nanoparticles.

### 3.7 Research on adsorption

#### 3.7.1 Kinetics of adsorption

Adsorption kinetics of Pb(II) and Cr(VI) ions onto MnO@SE nanocomposite was investigated using two widely used kinetic models: pseudo-first-order (PFO) and pseudo-second-order (PSO). These models describe various adsorption mechanisms and rate-controlling steps. Batch adsorption experiments were carried out with 0.6 g of MnO@SE and 25 mL of metal ion solutions Pb(II) and Cr(VI) at pH 2.0 and room temperature, as represented in Figure 6.

Within the first 30 minutes, the adsorption was rapid, showing the high concentration of active sites on MnO@SE's surface. This was followed by a slower but linear increase that occurred until equilibrium was attained after approximately 50 minutes with no additional significant gain in uptake thereafter. The kinetic model fitting parameters and their corresponding statistical equivalents are presented in Table 1. Among the models run, the PSO model gave the highest correlation coefficients ( $R^2 > 0.99$ ) for Pb(II) and ( $R^2 > 0.95$ ) for Cr(VI), suggests that the principal mechanism chemisorption [28]. This suggests that adsorption occurred through specific interactions such as surface complexation or ion exchange, and not through physical adsorption [29]. The adsorption capabilities at equilibrium computed from the PSO model were within a very close approximation of the experimentally found values, further justifying its suitability.

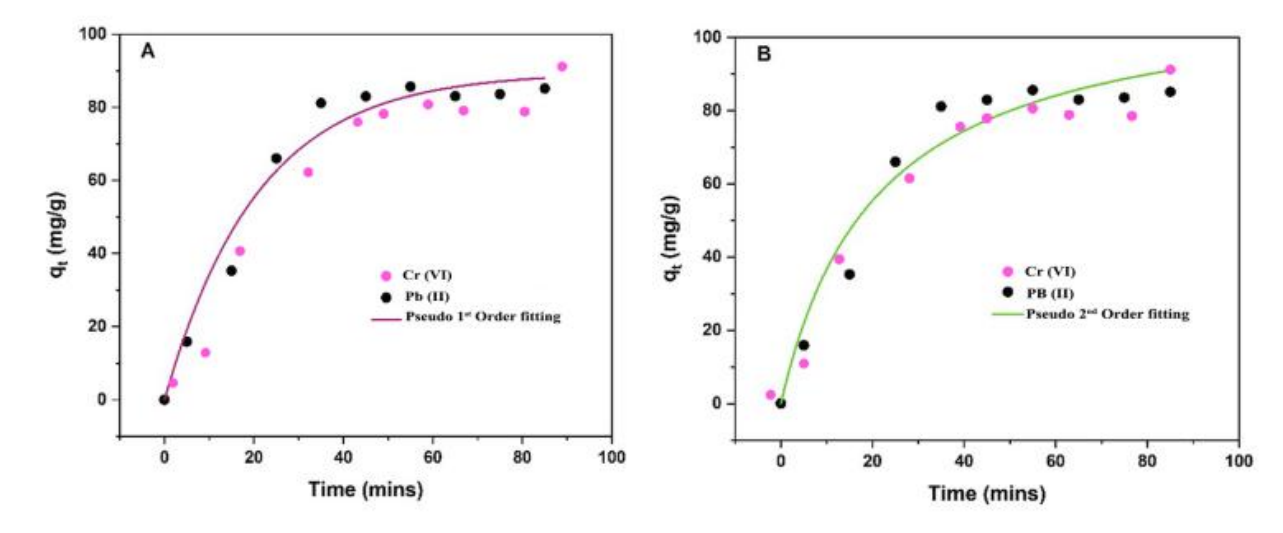


**Figure 6.** Adsorption kinetic models of MnO@SE on the removal of Pb(II) and Cr(VI) ions (A) Pseudo-first order, (B) Pseudo-second order

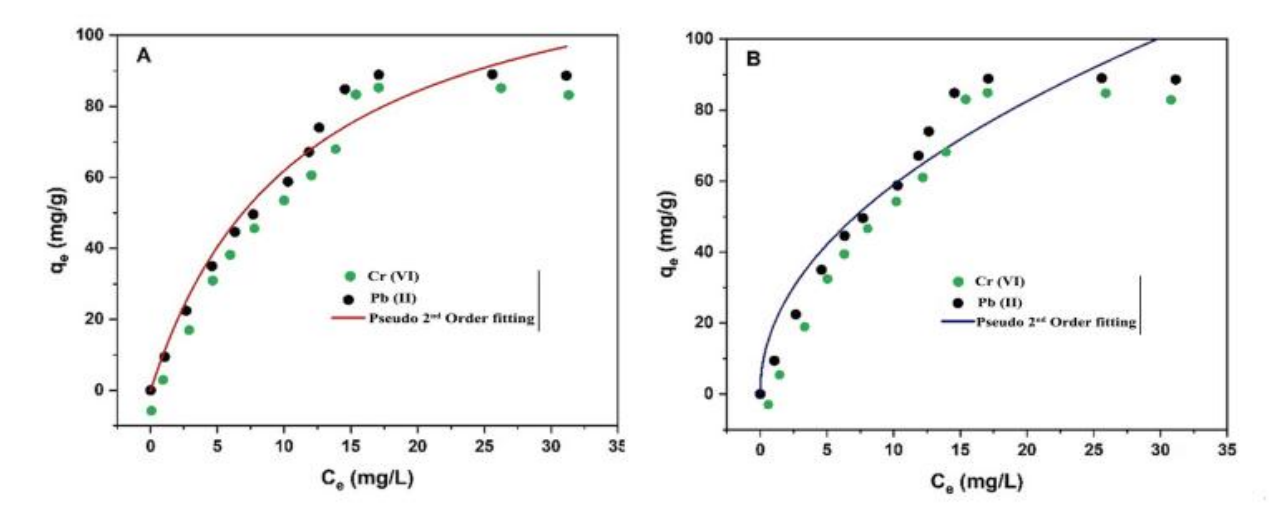


Figure 7. Adsorption isotherms for MnO@SE on the removal of Pb(II) and Cr(VI) ions (A) Langmuir model, (B) Freundlich model

**Table 1.** Adsorption kinetic models and parameters for Pb(II) and Cr(VI) adsorption on MnO@SE

Kinetic Models	Parameters -	Values		Adjusted R <sup>2</sup>		$\mathbb{R}^2$	
		Pb(II)	Cr(VI)	Pb(II)	Cr(VI)	Pb(II)	Cr(VI)
	Experimental q <sub>e</sub> (mg/g)	85.7	77.2	-	-	_	_
Pseudo-first order	$q_e (mg/g)$ $k_1 (min^{-1})$	81.5 0.048	70.67 0.032	0.9702	0.956	0.9735	0.945
Pseudo-second order	q <sub>e</sub> (mg/g) k <sub>2</sub> (mg/g·min)	113.5 0.0004	109.22 0.0003	0.9923	0.9768	0.9944	0.9554

**Table 2.** Adsorption isotherm model and parameters for Pb(II) and Cr(VI) adsorption on MnO@SE

Adsorption	Parameters -	Values		Adjusted R <sup>2</sup>		R <sup>2</sup>	
Models		Pb(II)	Cr(VI)	Pb(II)	Cr(VI)	Pb(II)	Cr(VI)
	Experimental q <sub>e</sub> (mg/g)	88.98	70	-	_	-	_
Lanamuir	$q_{max} (mg/g)$	132.18	99.22	0.9665	0.9543	0.9693	0.9555
Langmuir	$K_L (L/mg)$	0.088	0.789	_	_	_	_
Freundlich	$K_F (L/mg)$	19.31	11.23	0.9796	0.9643	0.9797	0.9641
ricultulich	n	2.06	1.90	_	_	_	_

### 3.7.2 Adsorption isotherms

To attain adsorption equilibrium, isotherm data were described by two models (Langmuir and Freundlich), as represented in Figure 7. Adsorption capacity of MnO@SE grew with the rise in initial concentrations of Pb(II) and Cr(VI), thereby ensuring strong adsorbate-adsorbent interactions. Isotherm fitting (Table 2) also indicated the Freundlich model to represent the experimental data with the highest values of R<sup>2</sup> (> 0.97) for Pb(II). The Freundlich model confirmed MnO@SE's heterogeneity and multilayer adsorption nature, Langmuir-like monolayer adsorption at concentration [30]. The Langmuir model gave maximum adsorption values (qmax) of ~132.18 mg g<sup>-1</sup> for Pb(II) and ~99.22 mg g<sup>-1</sup> for Cr(VI), which point towards the high binding potential of MnO@SE.

# 3.8 Cost implications of efficient green-synthesized adsorbents for wastewater treatment

Green synthesis technologies, particularly greensynthesized adsorbents, have strong potential for affordable wastewater treatment. For example, conventional activated sludge systems typically consume 0.3-0.6 kWh per m<sup>3</sup>— around \$0.04-\$0.08 per cubic meter of treatment [31]. Scaling this, treating 1 ton (~1 m³) of wastewater would cost approximately \$0.05. When combined with low-toxicity, renewable feedstocks, such green methods could reduce both energy and environmental costs—meriting further rigorous economic evaluation.

### 4. CONCLUSION

The green synthesis of the MnO@SE nanocomposite utilizing SE was successfully demonstrated in this study, as evidenced by FTIR, UV-Vis, EDX, XRD, and SEM analyses. Their high levels of Crystallinity allowed them to effectively adsorb Cr(VI) and Pb(II) ions. Purity and biogenic surface functionalization. Basically, at pH 2.0, 25 mg/L metal ion concentration, 0.2 g/L adsorbent dosage, and 50 minutes contact time, optimum adsorption was achieved with removal efficiencies above 98%. These findings highlight the possibility of environmentally friendly water treatment using MnO@SE nanocomposites. However, real-world applicability requires further validation, including regeneration studies, long-term performance trials, and kinetic/isotherm modelling.

Additional limitations include the unassessed impact of dissolved organic matter on adsorption efficiency, which could significantly influence performance in complex wastewater matrices. Moreover, organic matter interference has not been addressed. Future research should focus on regeneration and reuse studies, real wastewater application, and scale-up potential. Additionally, mechanistic insights via kinetic and isotherm modeling and toxicological assessments will further validate its environmental applicability and commercial viability.

### REFERENCES

- [1] Ali, I.Q., Kadhim, A.F., Latif, A.S., Al-Ibady, Q.A.N.A.K., Huno, S.H. (2025). Applications of bacterial biotechnology in the bioremediation of water contaminated with heavy metals. Agricultural Science Digest. https://doi.org/10.18805/ag.DF-694
- [2] Al-Ibady, Q.A.N.A.K., Hashim, A.K., Ghanim, S.A., Ajmi, R.N., Sayyid, M.M. (2025). Analysis of the effect of heavy elements in polluted industrial water and its environmental treatment: An applied study on the gas power plant/1 (central region) in southern Baghdad and its discharge into the Tigris River. International Journal of Environmental Impacts, 8(2): 415-421. https://doi.org/10.18280/ijei.080220
- [3] Nassrullah, S.A., Ismail, A.H., Al, Q.A.N.A.K., Al-Zuhairy, M.S., Farhan, A.A.R. (2025). Spatial and temporal variations of the water quality of Tigris River in north and south of Baghdad city. IOP Conference Series: Earth and Environmental Science, 1507(1): 012033. https://doi.org/10.1088/1755-1315/1507/1/012033
- [4] Aziz, M., Aziz, R., Rafiq, M.T., Abbasi, M., Taneez, M., Azhar, M.U., Askary, A.E., Elesawy, B.H., Eed, E.M., Khalifa, A.S., Qayyum, A. (2022). Efficient removal of lead and chromium from aqueous media using selenium based nanocomposite supported by orange peel. Frontiers in Environmental Science, 10: 947827. https://doi.org/10.3389/fenvs.2022.947827
- [5] Wei, Y., Yu, J., Haider, F.U., Zhang, Q., Chu, R., Liqun, C. (2025). Integrated removal of chromium, lead, and cadmium using nano-zero-valent iron-supported biochar: Mechanistic insights and eco-toxicity assessment. Ecotoxicology and Environmental Safety, 289: 117532. https://doi.org/10.1016/j.ecoenv.2024.117532
- [6] Li, L., Haziq, M.A., Ullah, S., Stanikzai, A.G., Bibi, S.D., Haq, T.U., Tayyeb, M., Yang, Z. (2024). Remediation of lead-contaminated water using green synthesized ironoxide nanoparticles: Performance and mechanism. Air, Soil and Water Research, 17: 11786221241278517. https://doi.org/10.1177/11786221241278517
- [7] Iravani, S. (2011). Green synthesis of metal nanoparticles using plants. Green Chemistry, 13(10): 2638-2650. https://doi.org/10.1039/C1GC15386B
- [8] Singh, P., Kim, Y.J., Zhang, D., Yang, D.C. (2016). Biological synthesis of nanoparticles from plants and microorganisms. Trends in Biotechnology, 34(7): 588-599. https://doi.org/10.1016/j.tibtech.2016.02.006
- [9] Ahmed, S., Ahmad, M., Swami, B.L., Ikram, S. (2016). A review on plants extract mediated synthesis of silver nanoparticles for antimicrobial applications: A green expertise. Journal of Advanced Research, 7(1): 17-28.

- https://doi.org/10.1016/j.jare.2015.02.007
- [10] Patra, J.K., Baek, K.H. (2014). Green nanobiotechnology: Factors affecting synthesis and characterization techniques. Journal of Nanomaterials, 2014(1): 417305. https://doi.org/10.1155/2014/417305
- [11] Khairy, G.M., Hesham, A.M., Jahin, H.E.S., El-Korashy, S.A., Awad, Y.M. (2022). Green synthesis of a novel eco-friendly hydrochar from pomegranate peels loaded with iron nanoparticles for the removal of copper ions and methylene blue from aqueous solutions. Journal of Molecular Liquids, 368: 120722. https://doi.org/10.1016/j.molliq.2022.120722
- [12] Afshin, S., Rashtbari, Y., Vosough, M., Dargahi, A., Fazlzadeh, M., Behzad, A., Yousefi, M. (2021). Application of Box-Behnken design for optimizing parameters of hexavalent chromium removal from aqueous solutions using Fe3O4 loaded on activated carbon prepared from alga: Kinetics and equilibrium study. Journal of Water Process Engineering, 42: 102113. https://doi.org/10.1016/j.jwpe.2021.102113
- [13] Monshi, A., Foroughi, M.R., Monshi, M.R. (2012). Modified Scherrer equation to estimate more accurately nano-crystallite size using XRD. World Journal of Nano Science and Engineering, 2(3): 154-160. https://doi.org/10.4236/wjnse.2012.23020
- [14] Ma, C., Sun, R., Chen, Y., Sun, J., Ji, H., Li, Y., Yang, G. (2020). Freeze-drying preparation of MnO x/graphene nanocomposite as anode material for highly reversible lithium storage. Journal of Materials Science, 55(13): 5545-5553. https://doi.org/10.1007/s10853-020-04395-y
- [15] Ijaz, F., Shahid, S., Khan, S.A., Ahmad, W., Zaman, S. (2017). Green synthesis of copper oxide nanoparticles using *Abutilon indicum* leaf extract: Antimicrobial, antioxidant and photocatalytic dye degradation activitie. Tropical Journal of Pharmaceutical Research, 16(4): 743-753. https://doi.org/10.4314/tjpr.v16i4.%x
- [16] Abdallah, Y., Ogunyemi, S.O., Abdelazez, A., Zhang, M., Hong, X., Ibrahim, E., Hossain, A., Fouad, H., Li, B., Chen, J. (2019). The green synthesis of MgO nanoflowers using Rosmarinus officinalis L.(rosemary) and the antibacterial activities against Xanthomonas oryzae pv. oryzae. BioMed Research International, 2019(1): 5620989. https://doi.org/10.1155/2019/5620989
- [17] Ma, Z., Wu, T., Li, P., Liu, M., Huang, S., Li, H., Zhang, Y., Yao, S. (2019). A dual (colorimetric and fluorometric) detection scheme for glutathione and silver (I) based on the oxidase mimicking activity of MnO2 nanosheets. Microchimica Acta, 186(8): 498. https://doi.org/10.1007/s00604-019-3613-4
- [18] Roy, H.S., Mollah, M.Y.A., Islam, M.M., Susan, M.A.B.H. (2018). Poly (vinyl alcohol)-MnO2 nanocomposite films as UV-shielding materials. Polymer Bulletin, 75(12): 5629-5643. https://doi.org/10.1007/s00289-018-2355-5
- [19] Ahmad, K.S., Yaqoob, S., Gul, M.M. (2022). Dynamic green synthesis of iron oxide and manganese oxide nanoparticles and their cogent antimicrobial, environmental and electrical applications. Reviews in Inorganic Chemistry, 42(3): 239-263. https://doi.org/10.1515/revic-2021-0033
- [20] Balakumar, V., Ryu, J.W., Kim, H., Manivannan, R., Son, Y.A. (2020). Ultrasonic synthesis of α-MnO<sub>2</sub> nanorods: An efficient catalytic conversion of refractory pollutant, methylene blue. Ultrasonics Sonochemistry, 62: 104870.

- https://doi.org/10.1016/j.ultsonch.2019.104870
- [21] Ijaz, I., Bukhari, A., Gilani, E., Nazir, A., Zain, H., Saeed, R. Hussain, S., Hussain, T., Bukhari, A., Naseer, Y., Aftab, R. (2022). Green synthesis of silver nanoparticles using different plants parts and biological organisms, characterization and antibacterial activity. Environmental Nanotechnology, Monitoring & Management, 18: 100704. https://doi.org/10.1016/j.enmm.2022.100704
- [22] Reddy, A.K., Jaisankar, V. (2019). Adsorption treatment of heavy metal removal from simulated wastewater using rice husk activated carbon (RHAC) and its polyvinylpyrrolidone (PVP) composite as an adsorbent. Journal of Water and Environmental Sciences, 3(1): 460-470
- [23] Hong, J., Xie, J., Mirshahghassemi, S., Lead, J. (2020). Metal (Cd, Cr, Ni, Pb) removal from environmentally relevant waters using polyvinylpyrrolidone-coated magnetite nanoparticles. RSC Advances, 10(6): 3266-3276. https://doi.org/10.1039/C9RA10104G
- [24] Adetokun, A.A., Uba, S., Garba, Z.N. (2019). Optimization of adsorption of metal ions from a ternary aqueous solution with activated carbon from acacia senegal (L.) willd pods using central composite design. Journal of King Saud University-Science, 31(4): 1452-1462. https://doi.org/10.1016/j.jksus.2018.12.007
- [25] Fakhar, N., Khan, S.A., Siddiqi, W.A., Khan, T.A. (2021). Ziziphus jujube waste-derived biomass as costeffective adsorbent for the sequestration of Cd2+from aqueous solution: Isotherm and kinetics studies. Environmental Nanotechnology, Monitoring & Management, 16: 100570. https://doi.org/10.1016/j.enmm.2021.100570

- [26] Somu, P., Kannan, U., Paul, S. (2019). Biomolecule functionalized magnetite nanoparticles efficiently adsorb and remove heavy metals from contaminated water. Journal of Chemical Technology & Biotechnology, 94(6): 2009-2022. https://doi.org/10.1002/jctb.5984
- [27] Madadgar, S., Doulati Ardejani, F., Boroumand, Z., Sadeghpour, H., Taherdangkoo, R., Butscher, C. (2023). Biosorption of aqueous Pb(II), Co (II), Cd (II) and Ni (II) ions from Sungun copper mine wastewater by Chrysopogon zizanioides root powder. Minerals, 13(1): 106. https://doi.org/10.3390/min13010106
- [28] Hu, M., Liu, L., Hou, N., Li, X., Zeng, D., Tan, H. (2021). Insight into the adsorption mechanisms of ionizable imidazolinone herbicides in sediments: Kinetics, adsorption model, and influencing factors. Chemosphere, 274: 129655. https://doi.org/10.1016/j.chemosphere.2021.129655
- [29] Zhang, B., Gao, B., Ma, W., Mo, Z., Song, Y., Xie, S., Jiang, F., Hu, X. (2023). Adsorption of uranium (VI) by natural vermiculite: Isotherms, kinetic, thermodynamic and mechanism studies. Journal of Environmental Radioactivity, 270: 107305. https://doi.org/10.1016/j.jenvrad.2023.107305
- [30] Yu, D., Wu, M., Hu, Q., Wang, L., Lv, C., Zhang, L. (2019). Iron-based metal-organic frameworks as novel platforms for catalytic ozonation of organic pollutant: Efficiency and mechanism. Journal of Hazardous Materials, 367: 456-464. https://doi.org/10.1016/j.jhazmat.2018.12.108
- [31] Porvoo Clean-Tech. (2024). Wastewater treatment prices | investment breakdown. https://porvoo.com.cn/blog/wastewater-treatment-prices-investment-breakdown/.